NANO LETTERS

Letter

pubs.acs.org/NanoLett

Epitaxy-Enabled Vapor–Liquid–Solid Growth of Tin-Doped Indium Oxide Nanowires with Controlled Orientations

Youde Shen,[†] Stuart Turner,[‡] Ping Yang,[§] Gustaaf Van Tendeloo,[‡] Oleg I. Lebedev,*[,∥] and Tom Wu*[,⊥]

[†]Division of Physics and Applied Physics, School of Physical and Mathematical Sciences, Nanyang Technological University, 637371, Singapore

[‡]EMAT, University of Antwerp, Groenenborgerlaan 171, B-2020 Antwerpen, Belgium

[§]Singapore Synchrotron Light Source (SSLS), National University of Singapore, 5 Research Link, 117603, Singapore

[∥]Laboratoire CRISMAT, ENSICAEN, CNRS UMR 6508, 6 Boulevard du Maréchal Juin, 14050 Caen, France

[⊥]Materials Science and Engineering, King Abdullah University of Science and Technology (KAUST), Thuwal 23955, Saudi Arabia

Supporting Information

ABSTRACT: Controlling the morphology of nanowires in bottom-up synthesis and assembling them on planar substrates is of tremendous importance for device applications in electronics, photonics, sensing and energy conversion. To date, however, there remain challenges in reliably achieving these goals of orientation-controlled nanowire synthesis and assembly. Here we report that growth of planar, vertical and randomly oriented tin-doped indium oxide (ITO) nanowires can be realized on yttria-stabilized zirconia (YSZ) substrates via the epitaxy-assisted vapor–liquid–solid (VLS) mechanism, by simply regulating the growth conditions, in particular the growth temperature. This robust control on nanowire orientation is facilitated by the small lattice mismatch of 1.6% between ITO and YSZ. Further control of the orientation, symmetry and shape of the nanowires can be achieved by using YSZ substrates with (110) and (111), in addition to (100) surfaces. Based on these insights, we succeed in growing regular arrays of planar ITO nanowires from patterned catalyst nanoparticles. Overall, our discovery of unprecedented orientation control in ITO nanowires advances the general VLS synthesis, providing a robust epitaxy-based approach toward rational synthesis of nanowires.

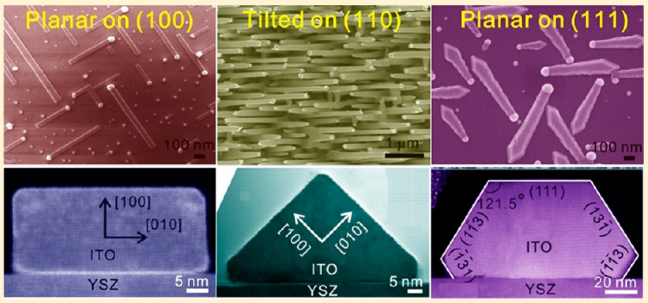

KEYWORDS: *Nanowire, indium tin oxide, vapor–liquid–solid mechanism, epitaxy, orientation control*

Nanowires (NWs) have been intensively explored for a wide range of applications in electronics,[1] photonics,[2] chemical/biological sensing,[3−5] and energy harvesting/conversion,[6−8] owing to their high surface-volume ratio and other remarkable properties.[9,10] Since the discovery of the vapor–liquid–solid (VLS) process in 1964 by Wagner and Ellis,[11] there have been many seminal works advancing NW synthesis and applications.[12−15] However, the large scale high-precision incorporation of as-grown out-of-plane NWs into nanodevices that often have planar configurations remains challenging. Most common approaches separate the NW growth and assembly steps, for example, harvesting and dispersing as-grown NWs in solution before casting them on substrates. To confront this bottleneck of NW assembly, various novel strategies such as the Langmuir–Blodgett technique,[16−18] blown-bubble method,[19] microfluidic alignment,[20] and microcontact printing[21,22] have also been developed. However, these approaches suffer from drawbacks such as imperfect alignment, mechanical damage, and solution contamination.

Recently, there are reports on in-plane grown NWs that can be directly incorporated in devices, eliminating the assembly step in fabrication.[23−32] In this approach, good lattice match between NW and substrate is a stringent requirement for the growth of planar NWs, and there are only limited examples in the literature. The majority of the previous reports regards wurtzite (hexagonal)-structured II–VI semiconductors, such as ZnO NWs on sapphire[24] or GaN[27] and GaN NWs on sapphire[29] or SiC.[31] Recently, some reports emerged on synthesis of planar III–V semiconductor NWs with zinc blende (cubic) structures, such as GaAs NWs on GaAs[25] and InAs NWs on GaAs.[26] Furthermore, self-aligned lateral NWs of In_2O_3, which is an important wide band gap oxide, were reported to grow on Si substrates.[23] However, the In_2O_3 NWs exhibited a semiellipsoidal cross section, indicating that the lattice mismatch as high as 7% and the amorphous SiO_2 layer at the In_2O_3/Si interface might compromise the synthesis of high quality NWs.

Regarding the growth mechanism, Zi and co-workers recently used a revised Gibbs–Thomson equation to illustrate that the growth of planar InAs NWs is energetically favored at

Received: March 29, 2014
Revised: June 9, 2014
Published: June 27, 2014

   dx.doi.org/10.1021/nl501163n | *Nano Lett.* 2014, 14, 4342−4351

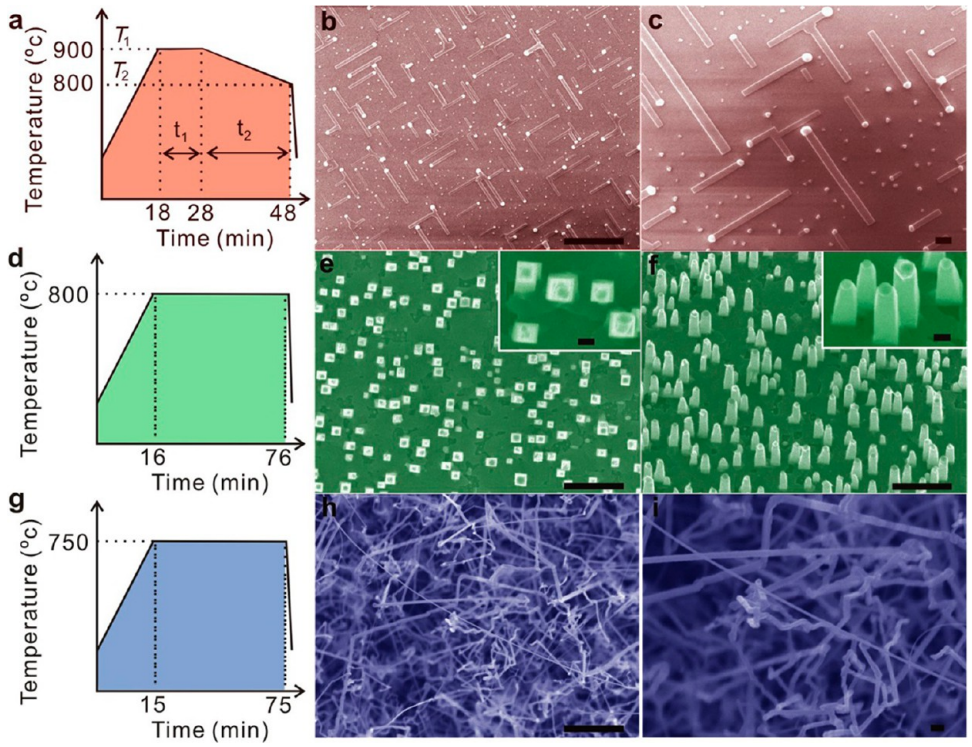

Figure 1. Synthesis of ITO NWs on (100) YSZ substrates. (a) Schematic illustration of the dynamic temperature profiles used in the synthesis of planar ITO NWs. (b,c) SEM images of planar NWs at different magnifications. (d) Schematic illustration of the growth conditions of vertical NWs. (e) SEM top-view image of vertical NWs. (f) SEM tilted view images of vertical NWs (tilt angle = 20°). Scale bars for the high-magnification images in (e,f) are both 100 nm. (g) Schematic illustration of the growth conditions of random NWs. (h,i) SEM images of random NWs with different magnifications. Scale bars are 1 μm in (b,e,f, h), and 100 nm in (c,i).

lower vapor pressures and smaller NW diameters.[33] On the dynamic aspect, Schwarz and Tersoff developed an anisotropic continuum model to capture the interplay between droplet statics and facet formation, and they successfully explained the anomalous kinking and crawling phenomena often observed in NW growth.[34−36]

In this work, we show that growth epitaxy and thermodynamics can be harnessed to enable unprecedented control of the orientation and morphology in tin-doped indium oxide (ITO) NWs. Because of their simultaneous high transparence and conductivity,[37] ITO NWs are promising for solar cells, displays, plasmonics, and LED applications.[38−47] In the previous works,[38−47] the transparent conducting nature of random and vertically aligned ITO NWs was confirmed and their device application was explored. Here we demonstrate a simple yet reliable strategy to grow not only random and vertically aligned ITO NWs but also planar ITO NWs on yttria-stabilized zirconia (YSZ) substrates by controlling the growth temperature profile. High-resolution transmission electron microscopy (HRTEM), electron diffraction (ED), high-angle annular dark-field scanning transmission electron microscopy (HAADF-STEM), annular bright-field STEM (ABF-STEM), and X-ray diffractometry (XRD) were used to investigate the structure of the as-fabricated NWs. We further leverage the epitaxial relationship between the ITO NWs and the YSZ substrate to realize a variety of ITO nanostructures with rich symmetry, orientation, and morphology. Our results advance the general VLS mechanism for NW growth, opening doors for the production of novel nanoarchitectures and devices.

Figure 1 shows the typical conditions of the vapor transport growth and the corresponding scanning electron microscopy (SEM) images of as-fabricated NWs on (100)-oriented YSZ substrates. The experimental details can be found in the Supporting Information and our previous works.[47−50] As shown in the temperature profile in Figure 1a, to grow in-plane NWs we first quickly raised the furnace tube to 900 °C, and stayed at 900 °C for 10 min before lowering the furnace temperature to 800 °C at a controlled rate. The whole growth process including the cooling down to room temperature takes roughly one and a half hours. Figure 1b,c shows the corresponding SEM images of as-fabricated planar NWs. We can clearly identify the Au nanoparticles at the apex of NWs, indicating that the NW growth follows the VLS process. XRD patterns (see Supporting Information Figure S1) confirm that these NWs are ITO with the cubic bixbyite crystal structure. Remarkably, the orientations of the planar NWs show 4-fold symmetry, which is a direct result of the crystallographic relationship between ITO NWs and YSZ substrate later confirmed by TEM. YSZ with a cubic structure is an ideal substrate for the growth of ITO NWs because of the small lattice mismatch, that is, $(2a_{YSZ} - a_{ITO})/a_{ITO} \sim 1.6\%$. Thus, the interface energy between ITO NWs and YSZ substrate will be the lowest when the ITO NWs grow epitaxially along specific [010] and [001] directions on the (100) YSZ surface. We also found in the SEM images that many tiny isolated Au particles with diameters smaller than 30 nm were still present on the substrate surface. Because of the Gibbs−Thomson effect,[51] these Au nanoparticles are likely too small to initiate the NW growth. Overall, the ITO NWs exhibit a width of 50 ± 9 nm, whereas the length has a much wider distribution between approximately 335 and 635 nm.

dx.doi.org/10.1021/nl501163n | *Nano Lett.* 2014, 14, 4342−4351

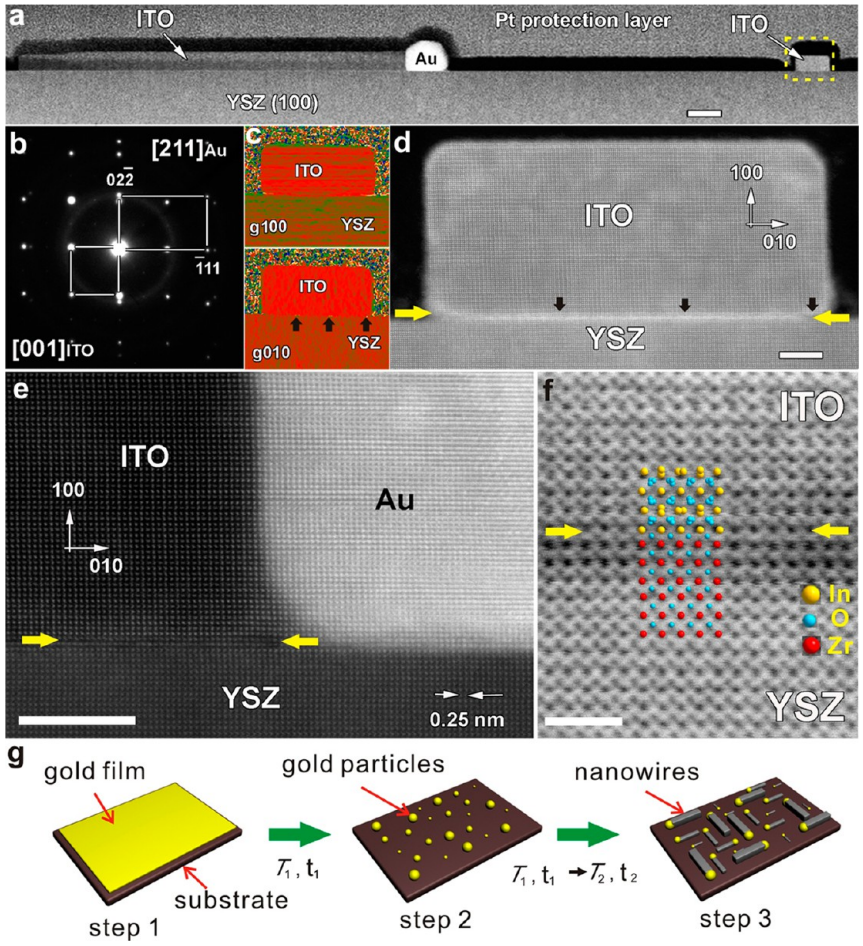

Figure 2. Structural characterization of planar ITO NWs. (a) Low-magnification HAADF-STEM image of planar ITO NWs on a (100) YSZ substrate. Scale bar, 50 nm. (b) SAED pattern taken from an area near the NW-catalyst interface, showing the epitaxial relationship between the ITO NW and the Au catalyst particle. The zone axis for the (S)TEM observation is noted. (c) Geometrical phase analysis data taken along the [100] and [010] directions of YSZ. (d) High-resolution ADF-STEM image of the cross-section of an ITO NW, which was taken at the area enclosed by dashed lines in (a). The white contrast at the interface indicates the presence of localized strain. Scale bar, 5 nm. The black arrows in (c,d) mark misfit dislocations at the interface. (e) High-resolution HAADF-STEM image of the trijunction of the ITO NW, the YSZ substrate, and the Au catalyst particle. Scale bar, 10 nm. (f) ABF-STEM image of the interface between the ITO NW and the YSZ substrate. Scale bar, 1 nm. In (d–f), the yellow arrows mark the ITO/YSZ interface. (g) Schematic illustration of the growth process of the planar ITO NWs.

Typical conditions for the growth of vertically aligned ITO NWs are consistent with previous reports.[39−41] In Figure 1d, a single growth temperature of 800 °C was used during a growth time of 1 h. The SEM top-view image in Figure 1e suggests square-shaped cross sections for the NWs with a uniform width of about 140 ± 18 nm and length of 980 ± 140 nm. The tilted view in Figure 1f shows that the ITO NWs exhibit a slightly tapered morphology and the Au nanoparticles are generally much smaller than the NW diameters, which is a result of the diffusion of Au catalyst during the VLS growth.[39]

When the growth temperature was further lowered to 750 °C (Figure 1g), we obtained random NWs without any preferred orientation. The SEM images in Figure 1h,i show that the NWs are no longer uniform and the majority of the NWs are not straight. The XRD data (Supporting Information Figure S1) indicate that the majority of the NWs have a crystal structure that is consistent with SnO_2, although some ITO NWs are still present. This is consistent with the fact that tin oxide can react with graphite and produce tin vapor at a lower temperature than indium oxide.[47] Thus, the formation of SnO_2 NWs is favored when the growth temperature is lower. Because SnO_2 NWs have a rutile structure (a = 4.750 Å and c = 3.198 Å), which does not match the structure of YSZ substrate (cubic, a = 5.150 Å), growth of random NWs is the natural result. Finally, the observation that no NWs grow at 700 °C and below may be a result of the limited reaction of the source mixture at low temperatures.

There are two immediate conclusions from the three runs of experiments shown in Figure 1: the first conclusion is that the highest temperature favors the growth of planar NWs, while NWs grow vertically at slightly lower temperatures, and randomly oriented NWs are observed at the lowest temperature of 750 °C; the second conclusion is that two temperature steps are required to grow planar NWs, which may be the reason why such planar ITO NWs were not discovered before. In order to better understand the growth process, we carried out about 100 runs of NW growth under systematic tuning of growth parameters, and Supporting Information Figure S2 summarizes the effect of growth temperature on the NW morphology. For the growth of planar NWs, we fixed the temperature T_1 and T_2 at 900 and 800 °C, respectively; the time duration t_1 at T_1 was fixed at 10 min, while the transition time t_2 was changed from 5 to 40 min. We found that the length of the NWs is controlled by the duration t_2, when the growth temperature is lowered

dx.doi.org/10.1021/nl501163n | Nano Lett. 2014, 14, 4342−4351

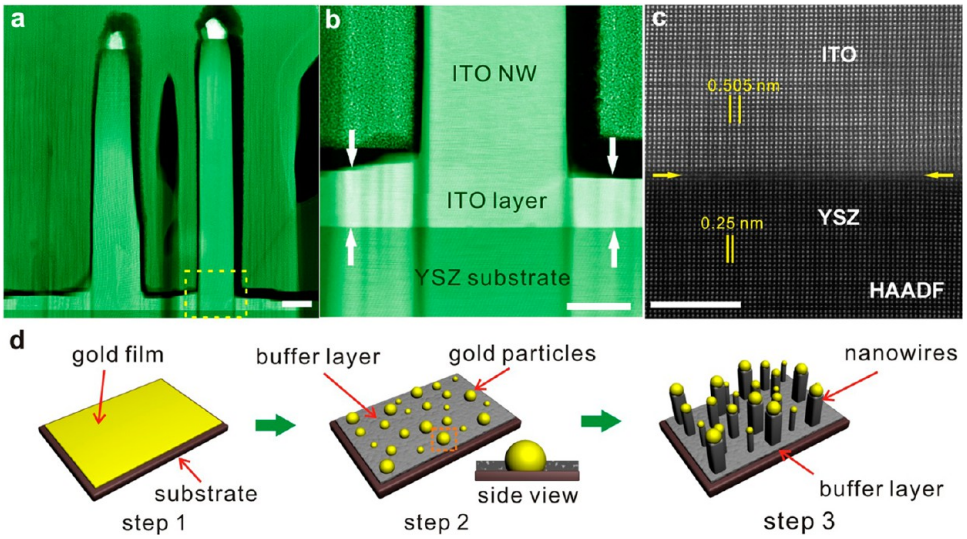

Figure 3. Characterization and growth mechanism of vertical ITO NWs. (a) Cross-sectional HAADF-STEM image of the out-of-plane ITO NWs. Scale bar, 100 nm. (b) High-magnification HAADF-STEM image for the marked rectangular area in (a). An epitaxial ITO layer with a thickness of ~40 nm, marked with white arrows, can be clearly seen on the YSZ substrate. Scale bar, 50 nm. (c) HAADF-STEM of the interface (marked by yellow arrows) between the ITO NW and the YSZ substrate. Scale bar, 5 nm. (d) Schematic illustration of the growth process of vertical ITO NWs, concurrent with the formation of a buffer layer.

from 900 to 800 °C, and the quasi-linear relationship is shown in Supporting Information Figure S3. On the other hand, when we fixed the temperature T_1, T_2 and time t_2, and changed t_1, the length of NWs remained nearly the same, but the number of planar NWs decreased with t_1 (see Supporting Information Figure S4). These results suggest that the planar NWs grow during the process of controlled cooling from 900 °C (T_1) to 800 °C (T_2). Without process t_2, no NWs grow (see Supporting Information Figure S2), which may be the result of the high decomposition/desorption rate of ITO in the reducing atmosphere at 900 °C. To verify this scenario, we kept a piece of ITO-coated substrate in the same growth environment, and the ITO film quickly decomposed and left residues on the substrate (see Supporting Information Figure S5). For the vertical NWs grown at 800 °C, the NW length linearly depends on the growth duration with a growth rate of about 8 nm/min (see Supporting Information Figure S6). The SEM images reveal the growth process: first a buffer layer forms on the surface of YSZ substrate, and the Au nanoparticles appear to be embedded in the buffer layer with limited lateral mobility, which may facilitate the out-of-plane growth.

We carried out extensive (S)TEM and reciprocal space mapping (RSM) experiments to investigate the crystalline structures of the planar, vertical, and random NWs as well as their growth mechanism. Figure 2a is a HAADF-STEM (Z-contrast) cross-section image of a planar NW. To prepare this type of cross-sectional samples, we applied the focused ion beam (FIB) lift-out technique. The bright-contrast Au catalyst particle can be identified at the top of the NW, confirming the SEM observation. As an important clue to the growth mechanism, we note that there is no buffer layer between the ITO NW and the YSZ substrate. In Figure 2b, a selected area ED (SAED) pattern taken near the Au/ITO interface suggests the following epitaxial relationships: $ITO_{[010]}//Au_{[-111]}$ and $ITO_{[001]}//Au_{[211]}$. Our TEM observations on several samples suggest that the NWs strictly grow along [010] and [001] directions, which explains the 4-fold symmetry observed in SEM experiments. Geometrical phase analysis (GPA) was applied to the acquired HRTEM images to investigate the deformation and strain state of the planar ITO NWs. The uniform color shown in Figure 2c indicates little deformation of ITO NW, and the small strain is homogeneously distributed. Figure 2d is a cross-section ADF-STEM image of a planar NW, showing the expected rectangular shape with slightly faceted corners. Furthermore, the strong diffraction contrast right at the interface of ITO and YSZ, together with the presence of misfit dislocations at the interface (black arrows) indicates heightened strain at the interface, but the lattice is almost fully relaxed inside the NW. In Figure 2e, a HAADF-STEM image taken at the ITO/YSZ/Au trijunction confirms the good epitaxial relationship between the ITO NW and the YSZ substrate. The ABF-STEM image in Figure 2f further reveals the excellent matched lattices at the ITO/YSZ interface. These observations shed light on the growth mechanism, and the process of growing planar NWs is illustrated in Figure 2g. At 900 °C, the absorption and desorption of precursor atoms are balanced on the bare YSZ surface, leading to no ITO film growth. However, as soon as the temperature lowers, the Au nanoparticles are effective in absorbing and retaining the precursor atoms for the subsequent ITO NW growth. In addition, the excellent lattice match between ITO and YSZ means that the interface energy is small, facilitating the in-plane growth.

In stark contrast to the in-plane case, the HAADF-STEM images in Figure 3a,b reveal vertical out-of-plane NW growth and the existence of an ITO buffer layer with a thickness of about 40 nm. In Figure 3c, the high-resolution HAADF-STEM image taken at the interface between an ITO NW and the YSZ substrate confirms the good epitaxial relationship between both. The buffer layer probably restricts the lateral movement of the Au catalyst nanoparticles on the bare YSZ surface, promoting the out-of-plane NW growth. As illustrated in the schematic in Figure 3d, the existence of such a buffer layer may be the critical factor triggering the out-of-plane growth of ITO NWs. In addition, a tin-rich phase ($InSnO_{3.5}$, so-called ISO phase) was

dx.doi.org/10.1021/nl501163n | Nano Lett. 2014, 14, 4342−4351

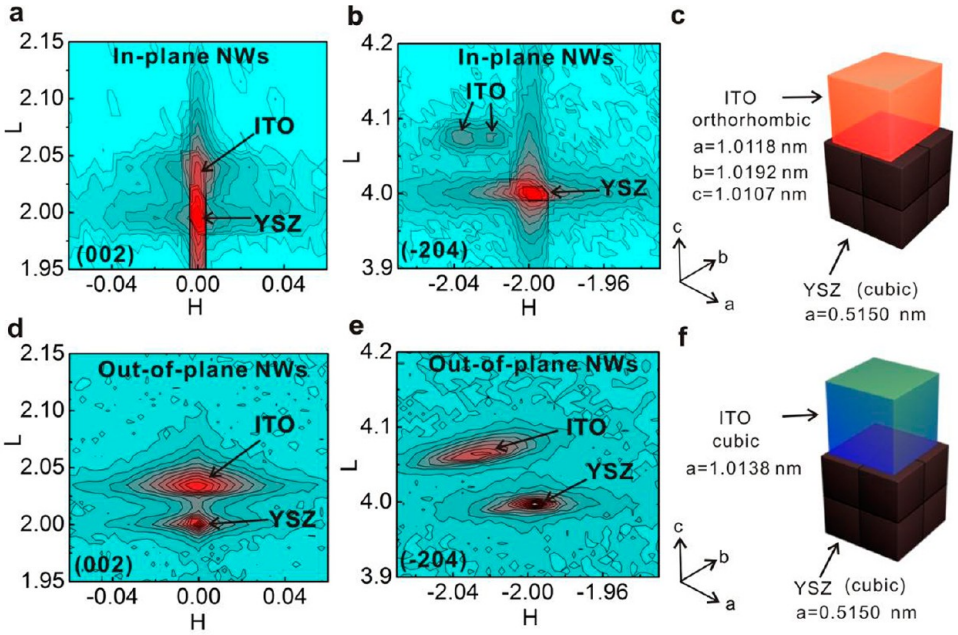

Figure 4. Reciprocal space maps of planar and vertical ITO NWs. (a,b) The (002) HL and (−204) HL reciprocal space mapping data of the planar ITO NWs grown on the (100) YSZ substrate. The (−204) KL mapping (not shown) has the same distribution of diffraction intensities as the HL mapping. (c) Schematic illustration of the deformed orthorhombic ITO unit cell on the cubic YSZ. For clarity, the structural deformation is exaggerated. For ITO NWs, there are two equivalent variants of deformation with orthogonal orientations. (d,e) The (002) HL and (−204) HL reciprocal space mapping data of the vertical ITO NWs grown on the (100) YSZ substrate. (f) Schematic illustration of the cubic structured ITO unit cell on the cubic YSZ substrate. The lattice constants for both planar and vertical ITO NWs were calculated from the coordinates of their diffraction peaks in the reciprocal space mapping data with the YSZ substrate as the reference.

also observed (see Supporting Information Figure S7), which is consistent with previous reports.[47,52]

The randomly oriented NWs clearly possess a more complicated and less controllable structure. Apart from the normal SnO_2 NWs with smooth surfaces (see Supporting Information Figure S8), two unusual zigzag and twin structures (see Supporting Information Figure S9) are also present. We attribute their formation to the low growth temperature. One reason is that more tin vapor will be generated than indium vapor at low temperature, which will change the normal ratio of In/Sn. The other reason is that defects are more easily formed at low temperature because of the lower mobility of the constituting atoms.

We further used the synchrotron-based RSM technique to precisely measure the crystalline structure and the strain state of the ITO NWs. Figure 4a shows the mapping data of the planar NWs near the (002) diffraction spot of the YSZ substrate, and the identical H value of the ITO ($L \sim 2.0380$) and YSZ ($L \sim 1.9998$) peaks indicate excellent alignment at the interface without any inclination. As shown in Figure 4b, the mapping data obtained near the (−204) diffraction spot reveal two ITO peaks with almost equal intensity. They can be attributed to the diffraction of two groups of planar NWs perpendicular to each other. Furthermore, the identical L value of both peaks indicates the same vertical lattice constant, whereas the different H values suggest difference in lateral lattice dimensions. We calculated the lattice constants of the planar ITO NWs as a = 10.118(5) Å, b = 10.192(5) Å, and c = 10.107(2) Å, which suggests an orthorhombic distortion of the ITO cubic structure. Comparing with the lattice constants of the bulk ITO materials (cubic bixbyite structure, a = 10.138 Å), we can conclude that the a and c axes of the planar NWs are slightly compressed while b axis is elongated. The schematic in Figure 4c illustrates the two equivalent deformation cases of ITO unit cells on the YSZ substrate, and the anisotropy of in-plane lattice parameters is apparently related to the NW growth. It is remarkable that the strain in the planar ITO NWs is anisotropic and smaller than 0.5%, even though the lattice mismatch between ITO and YSZ bulks is much larger at 1.6%, indicating effective stress relief in NWs.

Similarly, for the vertical NWs, the mapping data in Figure 4d at the (002) diffraction spot indicates no inclination between the NWs and the substrate. However, different from the in-plane case, the single (−204) peak for ITO in Figure 4e indicates that the vertical ITO NWs have the same a and b values. The lattice constants extracted from Figure 4d,e indicate that vertical ITO NWs are cubic structure with a constant of 10.138(2) Å. These results indicate that the mismatch strain is fully relaxed in the vertical NWs (Figure 4f), which differs from the case of planar NWs.

The success of using growth temperature as the single parameter to tune the orientation of ITO NWs on (100) YSZ substrates encouraged us to extend the method to the growth on (110) and (111) YSZ substrates with varied crystallographic symmetries. The growth conditions were kept the same as those used in the growth on (100) YSZ substrates. Figure 5a,b shows SEM and TEM images of planar ITO NWs on a (110) YSZ substrate. The planar NWs exhibit 4-fold symmetry, similar to the results obtained on (100) surface (see Figure 1b,c). However, careful SEM and TEM examinations revealed two types of cross-sectional shapes as shown in the inset of Figure 5a: The cross section of [001]-oriented NW is triangular, while that of [−110]-oriented NW is rectangular (Figure 5c). Furthermore, the TEM data in Supporting Information Figure S10a−c reveal that the two exposed facets of the triangular [001]-oriented NWs are (100) and (010)

dx.doi.org/10.1021/nl501163n | Nano Lett. 2014, 14, 4342−4351

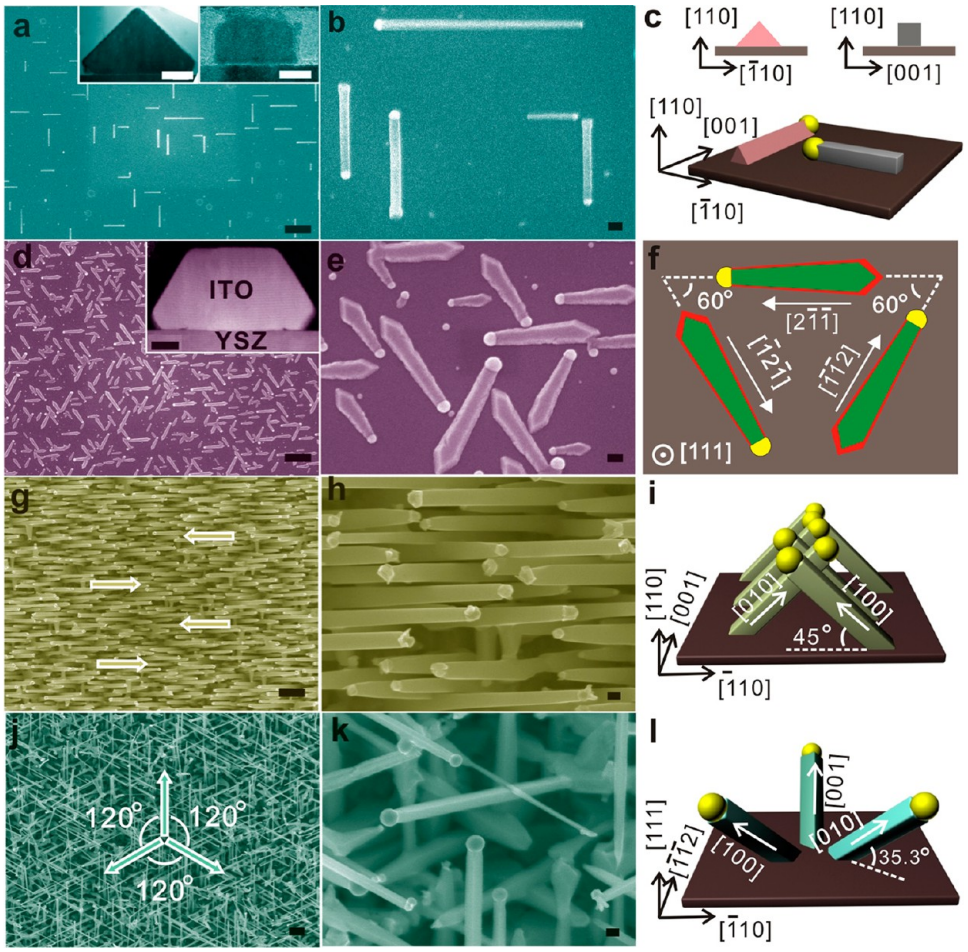

Figure 5. Aligned ITO NWs on (110) and (111) YSZ substrates. (a,b) SEM images of planar ITO NWs on a (110) YSZ substrate at different magnifications. The orientations of the NWs have a perpendicular configuration. The TEM images in (a) show the cross sections of ITO NWs observed along two directions: [001] and [−110]. (c) Schematic illustration of planar ITO NWs on a (110) YSZ substrate. The cross sections of the ITO NWs show triangular and rectangular shapes, depending on the orientation of the NWs. (d,e) SEM images of planar ITO NWs on (111) YSZ substrates at different magnifications. The orientations of the planar NWs have a 3-fold symmetry. The HAADF-STEM image in (d) shows the cross-section of NW. (f) Schematic illustration of planar ITO NWs on a (111) YSZ substrate. (g,h) SEM images of out-of-plane ITO NWs on a (110) YSZ substrate at different magnifications. The arrows in (g) indicate the orientations of NWs in the top-view. (i) Schematic illustration of the out-of-plane ITO NWs on a (110) YSZ substrate. (j,k) SEM image of out-of-plane ITO NWs on a (111) YSZ substrate at different magnifications. The arrows in (j) indicate the orientations of the NWs in the top view. (l) Schematic illustration of the out-of-plane ITO NWs on a (111) YSZ substrate. Scale bar, 1 μm in (a,d,g,j); 100 nm in (b,e,h,k); 20 nm in the insets of (a,d).

planes. Because the surface energy of {100}-type planes is lower than that of {110} planes,[53] the formation of {100} facets in NWs is favorable, leading to the triangular NW cross section. On the other hand, the cross section of [−110]-oriented NWs, shown in Supporting Information Figure S10d,e, is rectangular, which is similar to the cross section of NWs grown on (100) substrate in the second part (see Figure 2d). However, since the top plane of [−110]-oriented NWs is (110), which has a higher surface energy than (100), the top plane of [−110]-oriented NWs is not flat but split into small facets (see Supporting Information Figure S10f,g). The schematic diagram in Figure 5c summarizes the relationship between the ITO NWs and the (110) YSZ substrate.

Following the same dynamic profile of growth temperature as shown in Figure 1a, we also successfully synthesized planar ITO NWs on (111) YSZ substrates. As shown in the SEM images in Figure 5d,e, the orientations of such NWs exhibit a 3-fold symmetry. In Supporting Information Figure S11, cross-sectional TEM images of planar NWs on (111) YSZ are presented, and the substrate orientation and the surface terminations of NWs are determined. As a general rule, planar NWs always grow along the projected orientations of their preferred growth directions on the substrate surface.[54,55] It is well-known that for ITO NWs the preferred growth direction is the [100] group.[39,41,45,47] On the (111) plane, there are six equivalent projected directions of the [100] group: [1−21, [−12−1], [11−2], [−1−12], [−211], and [2−1−1]. However, because of the face-centered cubic crystal structure of YSZ, directions of [2−1−1], [−12−1], and [−1−12] are not equivalent to the other three (see Supporting Information Figure S12a,b). Remarkably, the observed 3-fold symmetry of the NWs implies that the ITO NWs prefer to grow along only three of the six directions. This reliable selection of growth orientations appears to be a result of energetic minimization of ITO-YSZ interfaces, and it clearly warrants further investigation.

Furthermore, the width of the NWs shrinks along the growth direction, producing a "tie"-like morphology in the top view. Once again, we applied the FIB sample preparation technique to cut the NWs and carried out the cross-sectional TEM

dx.doi.org/10.1021/nl501163n | *Nano Lett.* 2014, 14, 4342−4351

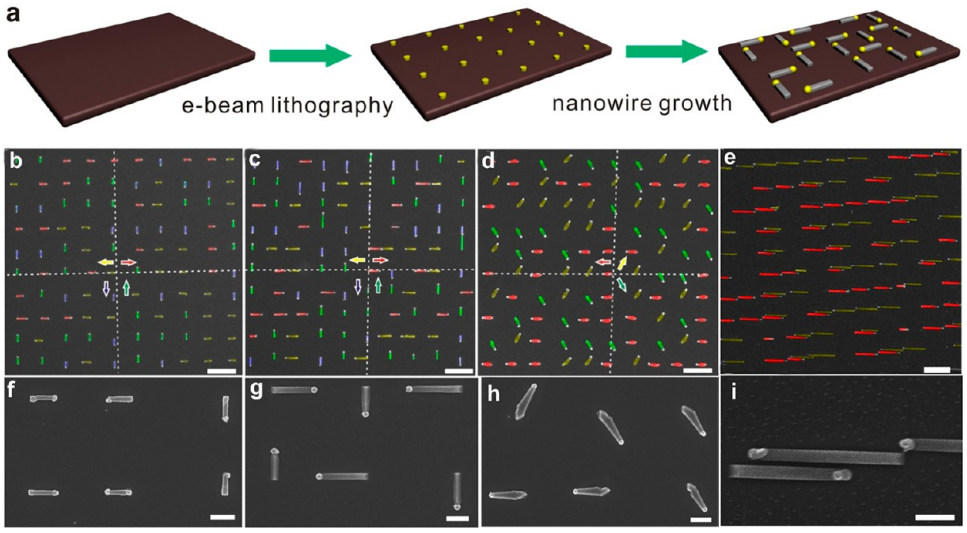

Figure 6. Regular arrays of planar ITO NWs. (a) Schematic illustration of site-specific planar ITO NWs grown from patterned Au catalyst nanoparticles. (b-d) SEM image of the as-fabricated NWs on (100), (110) and (111) YSZ substrates, respectively. The false colors of the NWs indicate the growth directions, that is, red, right; yellow, left; blue, down; and green, up in (b-c); red, left; yellow, right-up; and blue, right-down in (d). Examinations of dozens of SEM images suggest that the growth directions on various YSZ surfaces are equivalent within statistical errors. The growth directions of the ITO NWs further reveal the crystallographic axes of the YSZ substrate, which is about 3° tilted from coordinates of the EBL patterns of Au nanoparticles (marked by dashed lines). Scale bar, 5 μm. (e) SEM image of the as-fabricated NWs on (110) YSZ substrates, where the substrate with patterned Au catalyst was annealed at 900 °C for 1 h in air before the NW growth. The false colors of the NWs indicate the growth directions, that is, red, right; yellow, left. Scale bar, 5 μm. (f–i) SEM images of planar NW arrays with higher magnification. Scale bar, 1 μm.

studies. Interestingly, the cross section of these NWs transforms from a triangle to a trapezoid (Supporting Information Figure S11 and inset of Figure 5d) with increasing dimensions. The SAED pattern in Supporting Information Figure S11 reveals that the top surface of the trapezoid is (111), while the indexes of the side walls are (1−13) and (13−1). We summarize the growth habit of the planar ITO NW on (111) YSZ substrate in Figure 5f and Supporting Information Figure S12.

With the temperature profile shown in Figure 1d, aligned out-of-plane ITO NWs were grown on (110) and (111) YSZ substrates (Figure 5g–l). The good epitaxial relationship is similar to that in our previous report of ZnO NWs.[56] On the (110) YSZ substrate, there are two equivalent growth directions, that is, [100] and [010], making an angle of 45° with the substrate surface (Figure 5i). These NWs are perpendicular to each other in the side view but good alignment is achieved when projected on the (110) plane. While on the (111) YSZ substrate, there are three equivalent growth directions, that is, [100], [010], and [001], and the NWs form an angle of 35.3° with the substrate surface (Figure 5l). Similar to the (110) case, these three oriented NWs are perpendicular to each other; on the other hand, as shown in the SEM image in Figure 5j, an angle of 120° is formed when the NWs are projected onto the (111) YSZ surface.

In order to better control the dimensions and positioning of the NWs, we patterned the Au catalyst into square arrays of dots using electron beam lithography (EBL). The schematic of EBL patterning and NW growth processes is shown in Figure 6a. The diameter of the individual dots is 300 nm in Figure 6b,c, 500 nm in Figure 6d, and 400 nm in Figure 6e while the thickness is kept at 20 nm. The separation distance between the dots in the square arrays is 4 μm. As shown in the SEM images in Figure 6b–i, planar NW arrays with expected symmetries were successfully obtained on (100), (110), and (111) YSZ substrates. One advantage of this scheme is that the growth directions of the NWs can be precisely determined by examining the final positions of the nanoparticles relative to the original patterns. We found that all NWs grew exactly from the periodic square positions of the Au dots defined by EBL, suggesting that the Au nanoparticles did not migrate before the start of NW growth. Furthermore, the regular Au catalyst dots lead to ITO NWs with uniform dimensions, and the morphology control is apparently superior to the method of initiating growth with nanoparticles produced in thermal ripening of Au thin films.

As shown in Figure 6b,c, for the growth results obtained on (100) and (110) YSZ substrates, we used four different colors to highlight the growth directions. Our SEM examinations of over a dozen locations confirm that the four in-plane orientations are statistically equivalent. Similarly, we labeled the NWs grown on (111) YSZ substrate using three different colors (Figure 6d) and found roughly equal populations of these NW groups along three growth directions. Supporting Information Table S1 provides details on the length and width of the NWs. As expected, the NWs grown along four equivalent directions on the (100) YSZ substrate exhibit identical length and width (Figure 6f). Meanwhile, on the (110) YSZ substrate, the length of [−110]-oriented NWs with rectangular cross section (1.76 ± 0.31 μm) is notably larger than that of the [001]-oriented NWs with triangular cross section (1.36 ± 0.29 μm). The difference in length can also be seen in the high-magnification SEM images in Figure 6g, which indicates that the NW growth speed is higher along [−110] than that along [001]. Finally, the NWs on the (111) YSZ substrate show uniform tie-like morphology (Figure 6h), consistent with the fact that the three growth directions are equivalent. As a note on the side, uniform dispersed Au nanoparticles with controlled density can also be achieved by using polymer encapsulation that provides tailored electrostatic repulsion in a solution environment.[57] The use of this bottom-up strategy in future

dx.doi.org/10.1021/nl501163n | Nano Lett. 2014, 14, 4342−4351

research will enable the scale up synthesis of ITO NWs with controlled morphologies.

The fact that the orientation of ITO NWs on YSZ substrates, that is, planar, vertical, or random can be reliably realized by solely tailoring the growth temperature profile indicates the dominant role of thermodynamics in the NW synthesis. The epitaxial relationship between the ITO NWs and the YSZ substrate is the key to exploring the rich growth behaviors of NWs on YSZ substrates with (100), (110), and (111) surfaces. The mismatch between ITO and YSZ is only 1.6%, smaller than the cases of ZnO on GaN (1.8%),[27] InAs on GaAs (7.2%),[26] GaN on sapphire (16%),[29] and GaN on SiC (3.4%).[31] In the previous work on growing In_2O_3 nanowires on Si, the lattice mismatch is as large as 7%,[23] which compromises the synthesis of high-quality NWs. We also investigated the growth of ITO NWs on other crystalline substrates including sapphire, $SrTiO_3$ and Si, but the control of NW orientation is compromised due to the severe lattice mismatches (see Supporting Information Figure S13).

Conforming to the principles of energy minimization and interfacial epitaxy, ITO NWs exhibit triangular, rectangular or trapezoidal cross sections, as well as a novel "tie"-like morphology with dimension modulation along the length of NWs. In terms of crystalline structure, little deformation and few defects were detected in our systematic TEM experiments, and the effect of strain due to lattice mismatch is locally confined at the ITO/YSZ interface. Our RSM results show that the cubic lattice of bulk ITO transforms to an orthorhombic one with slight anisotropy in the planar NWs, while the small lattice mismatch exerts no influence at all on the out-of-plane vertical NWs. These features underscore the ITO/YSZ as one of the best systems available for investigating epitaxial growth of planar NWs.

On the thermodynamic aspect, Cao and Yang recently developed a theoretical model by introducing thermal fluctuation into the VLS process and concluded that higher growth temperatures tend to favor the growth of planar NWs.[58] This is consistent with our observation: regardless of the orientation of the YSZ substrate, the growth temperature of planar ITO NWis always higher than that of the vertical and random ones. Recently, Zi and co-workers used a revised Gibbs−Thomson equation to rationalize the planar growth of InAs NWs.[33] By treating a planar NW as a semicylindrical structure, they proposed that planar NW growth is favored by smaller Au nanoparticles.[33] In fact, on the (100) YSZ surface, we also found that the average diameter of the planar ITO NWs (50 ± 9 nm) is much smaller than that of the vertical ones (140 ± 18 nm), revealing the important role of the Gibbs−Thomson effect.

We should note that there are also kinetic factors at play in our experiments besides the conventional VLS mechanism: the time-dependent profile of growth temperature as shown in Figure 1 must be properly controlled in order to precisely control the NW orientation. Particularly, in the growth of vertical NWs the formation of ITO buffer layer is a concurrent process at the growth temperature of 800 °C and the confinement of catalyst nanoparticles dynamically guides the final orientation of NWs. Recently, in a study of planar ZnO NWs on sapphire, it was pointed out that the existence of ternary Au−ZnO−sapphire interfaces promotes the growth of horizontal growth.[59] In the case of planar ITO NWs, no ITO buffer layer forms at the growth temperature of 900 °C, and planar ITO NWs grow as the temperature gradually cools to 800 °C. In our case, good wetting of Au on both ITO and YSZ surfaces appears to be prerequisite for the growth of planar ITO NWs. Here we should mention that the extrinsic factors such as surface hydroxyl groups may not exert any significant influence on the NW growth under the experimental conditions used in our work. Recently, an in situ FT-IR spectroscopy and temperature-programed desorption study suggests that the removal of hydroxyl groups from the YSZ surface starts at modest annealing temperatures of 400−600 °C.[60] In our experiments, the growth and substrate temperatures are higher than 700 °C (Supporting Information Figure S14), thus the amount of surface hydroxyl groups is negligible on the YSZ surfaces.

A very recent theoretical study on faceted NW evolution demonstrated that the in-plane "crawling" growth mode, among multiple distinct modes of steady-state growth, can exist in a wide stability range.[36] Experimentally, we found that subtle adjustments of substrate and catalyst conditions can lead to drastic changes in the growth products. For example, after we annealed the (110) YSZ substrate with patterned Au catalyst at 900 °C for 1 h in air before the growth of NWs growth, the growth directions of ITO NWs decrease from four (Figure 6c,g) to two (Figure 6e,i). This refined selection of [−110]-oriented NWs with the rectangular cross section over [001]-oriented NWs with triangular cross section provides addition control on the growth orientation. Overall, the final growth morphology is the product of complex interplay of both thermodynamic factors like surface and interface energies and kinetic factors like initial phase nucleation and growth history.

Finally, regarding the applications of such morphology-controlled ITO nanowires, the vertical nanowires with a continuous layer underneath serve well as the bottom electrode for photoelectronic and photovoltaic devices, as already reported in some recent works.[42,61] On the other hand, the planar ITO nanowires with tailored shapes and orientations can be potentially used as miniature electrode for electronic and photonic nanodevices. We should mention that EDX mapping data of in-plane ITO NWs revealed a Sn concentration of 5−6 atom % (Supporting Information Figure S15), making such ITO nanowires suitable for applications as transparent conducting electrodes. It has also been demonstrated recently that the localized surface plasmon resonances of ITO nanorods in the infrared region can be modulated by ultraviolet light excitation;[62] the orientation-controlled ITO nanowires may find applications in telecommunication and sensing device. To produce large planar ITO nanowire arrays in a fast and large-scale manner, methods like imprint lithography can be employed.[63] We should also note that such morphology-controlled ITO nanowires can potentially be transferred to other supporting substrates if a suitable selective etching method can be found for the YSZ-ITO combination.[64]

In summary, the unprecedented freedom of producing NWs with diverse morphologies, as highlighted by this work, open doors toward not only the fabrication of advanced nanostructure and devices based on orientation-controlled NWs but also better understanding on the rich mechanisms of NW growth. Because ITO is the most widely used transparent conducting oxide, we expect that oriented ITO NWs will be applied to a wide range of solar and light-emitting nanodevices in future studies. Furthermore, the morphology control of ITO NWs and the epitaxy-based VLS growth mechanism are promising to be generalized to the synthesis of other NWs.

dx.doi.org/10.1021/nl501163n | Nano Lett. 2014, 14, 4342−4351

■ ASSOCIATED CONTENT

Supporting Information

The experimental details, XRD spectrum of as-made NWs, SEM images of control experiments, and TEM images of as-made NWs. This material is available free of charge via the Internet at http://pubs.acs.org.

■ AUTHOR INFORMATION

Corresponding Authors

*E-mail: (T.W.)Tao.Wu@KAUST.EDU.SA.
*E-mail: (O.I.L.) oleg.lebedev@ensicaen.fr.

Notes

The authors declare no competing financial interest.

■ ACKNOWLEDGMENTS

This work was supported in part by Singapore National Research Foundation, King Abdullah University of Science and Technology (KAUST), and European Union Seventh Framework Programme under Grant 312483 - ESTEEM2 (Integrated Infrastructure Initiative−I3). S.T. acknowledges the fund for scientific research Flanders (FWO) under the form of postdoctoral fellowship and for projects G004613N and G004413N. P.Y. is supported by SSLS via the NUS Core Support C-380-003-003-001.

■ REFERENCES

(1) Lu, W.; Lieber, C. M. *Nat. Mater.* **2007**, *6* (11), 841−850.
(2) Yan, R. X.; Gargas, D.; Yang, P. D. *Nat. Photonics* **2009**, *3* (10), 569−576.
(3) Rosi, N. L.; Mirkin, C. A. *Chem. Rev.* **2005**, *105* (4), 1547−1562.
(4) Zheng, G. F.; Patolsky, F.; Cui, Y.; Wang, W. U.; Lieber, C. M. *Nat. Biotechnol.* **2005**, *23* (10), 1294−1301.
(5) Cui, Y.; Wei, Q. Q.; Park, H. K.; Lieber, C. M. *Science* **2001**, *293* (5533), 1289−1292.
(6) Chan, C. K.; Peng, H. L.; Liu, G.; McIlwrath, K.; Zhang, X. F.; Huggins, R. A.; Cui, Y. *Nat. Nanotechnol.* **2008**, *3* (1), 31−35.
(7) Hochbaum, A. I.; Yang, P. D. *Chem. Rev.* **2010**, *110* (1), 527−546.
(8) Wang, Z. L.; Song, J. H. *Science* **2006**, *312* (5771), 242−246.
(9) Lieber, C. M.; Wang, Z. L. *MRS Bull.* **2007**, *32* (2), 99−108.
(10) Yang, P. D.; Yan, R. X.; Fardy, M. *Nano Lett.* **2010**, *10* (5), 1529−1536.
(11) Wagner, R. S.; Ellis, W. C. *Appl. Phys. Lett.* **1964**, *4* (5), 89−90.
(12) Morales, A. M.; Lieber, C. M. *Science* **1998**, *279* (5348), 208−211.
(13) Xia, Y. N.; Yang, P. D.; Sun, Y. G.; Wu, Y. Y.; Mayers, B.; Gates, B.; Yin, Y. D.; Kim, F.; Yan, Y. Q. *Adv. Mater.* **2003**, *15* (5), 353−389.
(14) Bierman, M. J.; Lau, Y. K. A.; Kvit, A. V.; Schmitt, A. L.; Jin, S. *Science* **2008**, *320* (5879), 1060−1063.
(15) Dayeh, S. A.; Picraux, S. T. *Nano Lett.* **2010**, *10* (10), 4032−4039.
(16) Whang, D.; Jin, S.; Wu, Y.; Lieber, C. M. *Nano Lett.* **2003**, *3* (9), 1255−1259.
(17) Kim, F.; Kwan, S.; Akana, J.; Yang, P. D. *J. Am. Chem. Soc.* **2001**, *123* (18), 4360−4361.
(18) Jin, S.; Whang, D. M.; McAlpine, M. C.; Friedman, R. S.; Wu, Y.; Lieber, C. M. *Nano Lett.* **2004**, *4* (5), 915−919.
(19) Yu, G. H.; Cao, A. Y.; Lieber, C. M. *Nat. Nanotechnol.* **2007**, *2* (6), 372−377.
(20) Huang, Y.; Duan, X. F.; Wei, Q. Q.; Lieber, C. M. *Science* **2001**, *291* (5504), 630−633.
(21) Ahn, J. H.; Kim, H. S.; Lee, K. J.; Jeon, S.; Kang, S. J.; Sun, Y. G.; Nuzzo, R. G.; Rogers, J. A. *Science* **2006**, *314* (5806), 1754−1757.
(22) Fan, Z. Y.; Ho, J. C.; Jacobson, Z. A.; Yerushalmi, R.; Alley, R. L.; Razavi, H.; Javey, A. *Nano Lett.* **2008**, *8* (1), 20−25.
(23) Hsin, C. L.; He, J. H.; Lee, C. Y.; Wu, W. W.; Yeh, P. H.; Chen, L. J.; Wang, Z. L. *Nano Lett.* **2007**, *7* (6), 1799−1803.
(24) Nikoobakht, B. *Chem. Mater.* **2007**, *19* (22), 5279−5284.
(25) Fortuna, S. A.; Wen, J. G.; Chun, I. S.; Li, X. L. *Nano Lett.* **2008**, *8* (12), 4421−4427.
(26) Zhang, X.; Zou, J.; Paladugu, M.; Guo, Y. A.; Wang, Y.; Kim, Y.; Joyce, H. J.; Gao, Q.; Tan, H. H.; Jagadish, C. *Small* **2009**, *5* (3), 366−369.
(27) Nikoobakht, B.; Herzing, A. *ACS Nano* **2010**, *4* (10), 5877−5886.
(28) Zhang, Z.; Wong, L. M.; Wang, H. X.; Wei, Z. P.; Zhou, W.; Wang, S. J.; Wu, T. *Adv. Funct. Mater.* **2010**, *20* (15), 2511−2518.
(29) Tsivion, D.; Schvartzman, M.; Popovitz-Biro, R.; von Huth, P.; Joselevich, E. *Science* **2011**, *333* (6045), 1003−1007.
(30) Nikoobakht, B.; Wang, X. D.; Herzing, A.; Shi, J. *Chem. Soc. Rev.* **2013**, *42* (1), 342−365.
(31) Tsivion, D.; Joselevich, E. *Nano Lett.* **2013**, *13* (11), 5491−5496.
(32) Bennett, P. A.; He, Z. A.; Smith, D. J.; Ross, F. M. *Thin Solid Films* **2011**, *519* (24), 8434−8440.
(33) Zi, Y. L.; Jung, K.; Zakharov, D.; Yang, C. *Nano Lett.* **2013**, *13* (6), 2786−2791.
(34) Schwarz, K. W.; Tersoff, J. *Phys. Rev. Lett.* **2009**, *102* (20), 206101.
(35) Schwarz, K. W.; Tersoff, J. *Nano Lett.* **2011**, *11* (2), 316−320.
(36) Schwarz, K. W.; Tersoff, J. *Nano Lett.* **2012**, *12* (3), 1329−1332.
(37) Mryasov, O. N.; Freeman, A. J. *Phys. Rev. B* **2001**, *64* (23), 233111.
(38) Wan, Q.; Song, Z. T.; Feng, S. L.; Wang, T. H. *Appl. Phys. Lett.* **2004**, *85* (20), 4759−4761.
(39) Wan, Q.; Dattoli, E. N.; Fung, W. Y.; Guo, W.; Chen, Y. B.; Pan, X. Q.; Lu, W. *Nano Lett.* **2006**, *6* (12), 2909−2915.
(40) Wan, Q.; Feng, P.; Wang, T. H. *Appl. Phys. Lett.* **2006**, *89* (12), 123102.
(41) Wan, Q.; Wei, M.; Zhi, D.; MacManus-Driscoll, J. L.; Blamire, M. G. *Adv. Mater.* **2006**, *18* (2), 234−238.
(42) O'Dwyer, C.; Szachowicz, M.; Visimberga, G.; Lavayen, V.; Newcomb, S. B.; Torres, C. M. S. *Nat. Nanotechnol.* **2009**, *4* (4), 239−244.
(43) Li, S. Q.; Guo, P. J.; Zhang, L. X.; Zhou, W.; Odom, T. W.; Seideman, T.; Ketterson, J. B.; Chang, R. P. H. *ACS Nano* **2011**, *5* (11), 9161−9170.
(44) Noh, J. H.; Han, H. S.; Lee, S.; Kim, J. Y.; Hong, K. S.; Han, G. S.; Shin, H.; Jung, H. S. *Adv. Energy Mater.* **2011**, *1* (5), 829−835.
(45) Gao, J.; Chen, R.; Li, D. H.; Jiang, L.; Ye, J. C.; Ma, X. C.; Chen, X. D.; Xiong, Q. H.; Sun, H. D.; Wu, T. *Nanotechnology* **2011**, *22* (19), 195706.
(46) Yu, H. K.; Dong, W. J.; Jung, G. H.; Lee, J. L. *ACS Nano* **2011**, *5* (10), 8026−8032.
(47) Gao, J.; Lebedev, O. I.; Turner, S.; Li, Y. F.; Lu, Y. H.; Feng, Y. P.; Boullay, P.; Prellier, W.; van Tendeloo, G.; Wu, T. *Nano Lett.* **2012**, *12* (1), 275−280.
(48) Guo, D. L.; Huang, X. A.; Xing, G. Z.; Zhang, Z.; Li, G. P.; He, M.; Zhang, H.; Chen, H. Y.; Wu, T. *Phys. Rev. B* **2011**, *83* (4), 045403.
(49) Wang, D. D.; Xing, G. Z.; Gao, M.; Yang, L. L.; Yang, J. H.; Wu, T. *J. Phys. Chem. C* **2011**, *115* (46), 22729−22735.
(50) Wang, D. D.; Chen, Q.; Xing, G. Z.; Yi, J. B.; Bakaul, S. R.; Ding, J.; Wang, J. L.; Wu, T. *Nano Lett.* **2012**, *12* (8), 3994−4000.
(51) Givargizov, E. I. *J. Cryst. Growth* **1975**, *31* (Dec), 20−30.
(52) Meng, G.; Yanagida, T.; Nagashima, K.; Yoshida, H.; Kanai, M.; Klamchuen, A.; Zhuge, F. W.; He, Y.; Rahong, S.; Fang, X. D.; Takeda, S.; Kawai, T. *J. Am. Chem. Soc.* **2013**, *135* (18), 7033−7038.
(53) Hao, Y. F.; Meng, G. W.; Ye, C. H.; Zhang, L. D. *Cryst. Growth Des.* **2005**, *5* (4), 1617−1621.
(54) Fortuna, S. A.; Li, X. L. *Semicond. Sci. Technol.* **2010**, *25* (2), 024005.
(55) Dowdy, R. S.; Walko, D. A.; Li, X. L. *Nanotechnology* **2013**, *24* (3), 035304.

(56) Li, G. P.; Jiang, L.; Wang, S. J.; Sun, X. W.; Chen, X. D.; Wu, T. *Cryst. Growth Des.* **2011**, *11* (11), 4885−4891.
(57) Guo, D. L.; Tan, L. H.; Wei, Z. P.; Chen, H. Y.; Wu, T. *Small* **2013**, *9* (12), 2069−2075.
(58) Cao, Y. Y.; Yang, G. W. *J. Phys. Chem. C* **2012**, *116* (10), 6233−6238.
(59) Nikoobakht, B.; Eustis, S.; Herzing, A. *J. Phys. Chem. C* **2009**, *113* (17), 7031−7037.
(60) Kogler, M.; Kock, E. M.; Bielz, T.; Pfaller, K.; Klotzer, B.; Schmidmair, D.; Perfler, L.; Penner, S. *J. Phys. Chem. C* **2014**, *118* (16), 8435−8444.
(61) Han, H. S.; Kim, J. S.; Kim, D. H.; Han, G. S.; Jung, H. S.; Noh, J. H.; Hong, K. S. *Nanoscale* **2013**, *5* (8), 3520−3526.
(62) Tice, D. B.; Li, S. Q.; Tagliazucchi, M.; Buchholz, D. B.; Weiss, A. W.; Chang, P. C. *Nano Lett.* **2014**, *14* (3), 1120−1126.
(63) Jung, G. Y.; Johnston-Halperin, E.; Wu, W.; Yu, Z. N.; Wang, S. Y.; Tong, W. M.; Li, Z. Y.; Green, J. E.; Sheriff, B. A.; Boukai, A.; Bunimovich, Y.; Heath, J. R.; Williams, R. S. *Nano Lett.* **2006**, *6* (3), 351−354.
(64) Goren-Ruck, L.; Tsivion, D.; Schvartzman, M.; Popovitz-Biro, R.; Joselevich, E. *ACS Nano* **2014**, *8* (3), 2838−2847.

dx.doi.org/10.1021/nl501163n | *Nano Lett.* 2014, 14, 4342−4351